

Running title: Advanced lesion symptom mapping analyses

## **Advanced lesion symptom mapping analyses and implementation as BCBtoolkit**

Foulon C<sup>a,b,c\*</sup>, Cerliani L<sup>a,b,c</sup>, Kinkingnéhun S<sup>a</sup>, Levy R<sup>b</sup>, Rosso C<sup>c,d</sup>, Urbanski M<sup>a,b,c</sup>, Volle E<sup>a,b,c</sup>, Thiebaut de Schotten M<sup>a,b,c\*</sup>

<sup>a</sup> Brain Connectivity and Behaviour Group, Brain and Spine Institute, Paris France.

<sup>b</sup> Frontlab, Institut du Cerveau et de la Moelle épinière (ICM), UPMC UMRS 1127, Inserm U 1127, CNRS UMR 7225, Paris, France.

<sup>c</sup> Centre de Neuroimagerie de Recherche CENIR, Groupe Hospitalier Pitié-Salpêtrière, Paris, France.

<sup>d</sup> APHP, Urgences Cérébro-Vasculaires, Groupe Hospitalier Pitié-Salpêtrière, Paris, France.

\* Corresponding authors [hd.chrisfoulon@gmail.com](mailto:hd.chrisfoulon@gmail.com) and [michel.thiebaut@gmail.com](mailto:michel.thiebaut@gmail.com)

Running title: Advanced lesion symptom mapping analyses

**Abstract:** Patients with brain lesions provide a unique opportunity to understand the functioning of the human mind. However, even when focal, brain lesions have local and remote effects that impact functionally and structurally connected circuits. Similarly, function emerges from the interaction between brain areas rather than their sole activity. For instance, category fluency requires the association between executive, semantic and language functions. Here we provide, for the first time, a set of complementary solutions to measure the impact of a given lesion upon the neuronal circuits. Our methods, which were applied to 37 patients with a focal frontal brain lesion, revealed a large set of directly and indirectly disconnected brain regions that had significantly impacted category fluency performance. The directly disconnected regions corresponded to areas that are classically considered as functionally engaged in verbal fluency and categorization tasks. These regions were also organized into larger directly and indirectly disconnected functional networks, including the left ventral fronto-parietal network, whose cortical thickness correlated with performance on category fluency. The combination of structural and functional connectivity together with cortical thickness estimates reveal the remote effects of brain lesions, provide for the identification of the affected networks and strengthen our understanding of their relationship with cognitive and behavioural measures. The methods presented are available and freely accessible in the *BCBtoolkit* as supplementary software (<http://toolkit.bcblab.com>).

## Running title: Advanced lesion symptom mapping analyses

Recent advances in neuroimaging techniques, allowed for the further examination of the structural and the functional organization of the human brain. While diffusion weighted imaging (DWI) tractography (Jones *et al.*, 1999) depicts how brain areas are connected together, functional magnetic resonance imaging (fMRI) measures the activity within and interaction between brain areas in the elaboration of function (Logothetis, 2008). These methods have been successfully applied to the healthy human brain, however, they remain underused in patients with brain lesions.

Patients with brain lesions provide a unique opportunity to understand the functioning of the human mind. Lesion symptom mapping analyses traditionally assume that visible and directly damaged areas are responsible for a patient's symptoms (Broca, 1861; Damasio and Damasio, 1989; Rorden *et al.*, 2007; Mah *et al.*, 2014). Following this logic, the areas that are the most frequently damaged by the lesion are considered as the neuronal substrate for the function. Previous studies employing this method have pinpointed critical areas dedicated to, for example, language production (Bates *et al.*, 2003), comprehension (Dronkers *et al.*, 2004), spatial awareness (Husain and Kennard, 1996; Karnath *et al.*, 2001; Mort *et al.*, 2003; Bird *et al.*, 2006) and other high-level cognitive functions (Coulthard *et al.*, 2008; Volle *et al.*, 2008; Badre *et al.*, 2009; Volle *et al.*, 2013). However, anatomical disconnections between regions are also important considerations for the exploration of cognitive deficit (Geschwind, 1965a, b). The dysfunction of distant areas that are connected to the lesioned tissue have also been reported in fMRI studies. They have shown that the networks are disrupted even by distant lesions through disconnection and diaschisis mechanisms (Finger *et al.*, 2004; Corbetta *et al.*, 2005; Carrera and Tononi, 2014).

Non-local effects of lesions have previously been explored using various forms of atlas-based analyses of tract damage (Rudrauf *et al.*, 2008; Thiebaut de Schotten *et al.*, 2008; Fridriksson *et al.*, 2013; Thiebaut de Schotten *et al.*, 2014; Corbetta *et al.*, 2015; Cazzoli *et al.*, 2016; Hope *et al.*, 2016; Urbanski *et al.*, 2016; Griffis *et al.*, 2017; Piai *et al.*, 2017), lesion-driven tractography (He *et al.*, 2007; Turken and Dronkers, 2011; Griffis *et al.*, 2017), disconnectome-mapping (Bonilha *et al.*, 2015; Thiebaut de Schotten *et al.*, 2015; Kuceyeski *et al.*, 2016; Yourganov *et al.*, 2016) and lesion-driven resting state fMRI (rs-fMRI) connectivity (Turken and Dronkers, 2011; Boes *et al.*, 2015). However, determining what

Running title: Advanced lesion symptom mapping analyses

these methods actually measure and identifying how to properly combine them are not always fully clear to the scientific community. Furthermore, there is an extremely limited availability of free, open-source software that applies methods to measure the non-local effects of lesions. These resources and scientific tools remain very much inaccessible and present a potential threat to reproducible science (Munafo, 2017).

Disconnections and diaschisis can have an impact upon distant regions in several respects through maladaptive responses and pathological spread (Fornito *et al.*, 2015). When disconnected from its inputs and outputs, a region can no longer contribute to the elaboration of the supported function. This phenomenon is called diaschisis (Feeney and Baron, 1986; Finger *et al.*, 2004; Carrera and Tononi, 2014). Once deprived from its inputs and/or outputs, transneuronal degeneration in the region will occur (Fornito *et al.*, 2015), dendrites and synapses density will decrease in number, myelin content will be altered and neurons will reduce in size or die through a mechanism called apoptosis, a programmed cell death (Cowan, 1970; Bredesen, 1995; Capurso *et al.*, 1997). Hence, a white matter disconnection leads to both functional and anatomical changes that extend well beyond the visible damage. New approaches are therefore required to capture the long-range effects that follow brain disconnections. For instance, cortical thickness (e.g. Schaechter *et al.*, 2006) and other volumetric (e.g. voxel based morphometry Xing *et al.*, 2016) analyses have been previously used to study the structural changes associated with brain lesions, but have not been applied in the context of brain disconnection.

In response to this need, we provide here a set of complementary solutions to measure both the circuit, and the subsequent change within the circuit that is caused by a lesion. We applied these methods to 37 patients with a focal brain lesion following a stroke or a surgical resection. We first assessed the risk of disconnection in well-known white matter tracts and tested their relationship with category fluency performance. Category fluency is an appropriate test to explore disconnection since it requires the association between executive, semantic and language functions (Gladsjo *et al.*, 1999; MacPherson and Della Sala, 2015). We then developed a tractography-based approach in order to produce maps of the areas that are directly disconnected by the lesion and tested their relationship with category fluency performance. We additionally calculated the rs-fMRI connectivity of these areas to reveal the

Running title: Advanced lesion symptom mapping analyses

whole network of directly and indirectly connected regions that participate in category fluency. Finally, we explored potential microstructural changes in the latter disconnected regions, by estimating neuronal loss or local connectivity degeneration derived from MR-based measures of cortical thickness and resting state *f*MRI entropy.

## Methods

### *Participants and Category fluency task*

Thirty-seven right-handed patients (French-native speakers; 19 females; mean age  $48 \pm 14.2$  years, age ranging from 23 to 75 years) who presented with a frontal lobe lesion at the chronic stage ( $> 3$  months) were included in this study (see table 1 for demographics). These patients were recruited from the stroke unit and the neuroradiology department at Salpêtrière Hospital, the neurological unit at Saint-Antoine Hospital and the neuroradiology department at Lariboisière Hospital in Paris. Patients with a history of psychiatric or neurological disease, drug abuse, or MRI contraindications were not included. Additionally, we gathered behavioural data from 54 healthy participants (French-native speakers; 27 females; mean age  $45.8 \pm 14.4$  years, age ranging from 22 to 71 years) in order to constitute a normative group. All participants performed a category fluency task (Lezak, 1995) in French. They were instructed to name as many animals as quickly as possible during a timed period of 60 seconds. The results were recorded by a clinical neuropsychologist (M.U.). Repetition and declination of the same animal were not taken into account in the final category fluency score.

The experiment was approved by the local ethics committee; all participants provided written informed consent in accordance to the Declaration of Helsinki. Participants also received a small indemnity for their participation.

### *Magnetic resonance imaging*

An axial three-dimensional magnetization prepared rapid gradient echo (MPRAGE) dataset covering the whole head was acquired for each participant (176 slices, voxel resolution =  $1 \times 1 \times 1$  mm, echo time = 3 msec, repetition time = 2300 msec, flip angle =  $9^\circ$ ).

Additionally, the same participants underwent a *f*MRI session of resting state. During the

## Running title: Advanced lesion symptom mapping analyses

resting state session, participants were instructed to relax, keep their eyes closed but to avoid falling asleep. Functional images were obtained using T2-weighted echo-planar imaging (EPI) with blood oxygenation level-dependent contrast using SENSE imaging an echo time of 26 msec and a repetition time of 3000 msec. Each dataset comprised 32 axial slices acquired continuously in ascending order covering the entire cerebrum with a voxel resolution of  $2 \times 2 \times 3$  mm. 200 volumes were acquired using these parameters for a total acquisition time of 10 minutes.

Finally, diffusion weighted imaging was also acquired for 10 participants of the normative group (French-native male speakers; mean age  $56.44 \pm 10$  years, age ranging from 45 to 66 years) and consisted in a total of 70 near-axial slices acquired using a fully optimised acquisition sequence for the tractography of diffusion-weighted imaging (DWI), which provided isotropic ( $2 \times 2 \times 2$  mm) resolution and coverage of the whole head with a posterior-anterior phase of acquisition. The acquisition was peripherally-gated to the cardiac cycle (Jones *et al.*, 2002) with an echo time = 85 msec. We used a repetition time equivalent to 24 RR. At each slice location, 6 images were acquired with no diffusion gradient applied. Additionally, 60 diffusion-weighted images were acquired, in which gradient directions were uniformly distributed on the hemisphere with electrostatic repulsion. The diffusion weighting was equal to a b-value of  $1500 \text{ sec mm}^{-2}$ .

### *Stereotaxic space registration*

As spatial normalisation can be affected by the presence of a brain lesion, additional processing was required before calculating the normalisation. To this purpose, the first step was to produce an enantiomorphic filling of the damaged area (Nachev *et al.*, 2008). Each patient lesions (or signal abnormalities due to the lesion) were manually segmented (using FSLview; <http://fsl.fmrib.ox.ac.uk>) and replaced symmetrically by the healthy tissue of the contralateral hemisphere. Enantiomorphic T1 images were fed into FAST (Zhang *et al.*, 2001) for estimation of the bias field and subsequent correction of RF inhomogeneity. This improved the quality of the automated skull stripping performed using bet (Smith, 2002) and the registration to the MNI152 using affine and diffeomorphic deformations (Avants *et al.*, 2011). The original T1 images (non enantiomorphic) were registered to the MNI152 space using the same affine and diffeomorphic deformations as calculated above. Subsequently, lesions were segmented again in the MNI152 space under the supervision of an expert

Running title: Advanced lesion symptom mapping analyses

neurologist (E.V.). This method has been made freely available as the tool *Normalisation* as part of *BCBtoolkit* (<http://toolkit.bcblab.com>).

### *White matter tracts disconnection*

Each patient's lesion was compared with an atlas of white matter tracts (Rojkova *et al.*, 2016), indicating for each voxel, the probability of finding a white matter tract such as the arcuate fasciculus, the frontal aslant tract or the uncinate fasciculus in the MNI152 coordinate system. We considered a tract to be involved when the likelihood of a tract being present in a given voxel was estimated above 50% (Thiebaut de Schotten *et al.*, 2014). This method is freely available as *tractotron* in *BCBtoolkit* (<http://toolkit.bcblab.com>). We focused on frontal lobe tracts with a potential effect on executive, semantic and language functions since all of the patients had a frontal lesion. These tracts included the cingulum, frontal aslant and the frontal superior and inferior longitudinal tracts for the executive functions (Catani *et al.*, 2012), the uncinate and the inferior fronto-occipital fasciculi for the semantic access (Duffau *et al.*, 2005; Von Der Heide *et al.*, 2013) and the anterior and long segment of the arcuate fasciculi for the phonemic system (Catani *et al.*, 2005; Catani and Bambini, 2014). A Kruskal Wallis test was employed to compare performance on the category fluency test for each tract between both preserved and disconnected patients and control participants. Subsequently, for each significant tract between patients Mann Whitney post-hoc comparisons were performed (**Fig. 1**).

### *Direct disconnection of brain areas: structural connectivity network*

This approach employed the diffusion weighted imaging datasets of 10 participants in the normative group to track fibers passing through each lesion. For each participant, tractography was estimated as indicated in (Thiebaut de Schotten *et al.*, 2011a).

Patients' lesions in the MNI152 space were registered to each control native space using affine and diffeomorphic deformations (Avants *et al.*, 2011), and subsequently, used as seed for the tractography in Trackvis (<http://trackvis.org>). Tractography from the lesions were transformed in visitation maps (Ciccarelli *et al.*, 2003; Thiebaut de Schotten *et al.*, 2011b), binarised and brought to the MNI152 using the inverse of precedent deformations. Finally, we produced a percentage overlap map by summing at each point in MNI space the normalized visitation map of each healthy subject. Hence, in the resulting disconnectome

Running title: Advanced lesion symptom mapping analyses

map, the value in each voxel took into account the inter-individual variability of tract reconstructions in controls, and indicated a probability of disconnection from 50 to 100% for a given lesion. This procedure was repeated for all lesions, allowing the construction of a disconnectome map for each patient/lesion. These steps were automatized in the tool *disconnectome map* as parts of the BCBtoolkit.

Thereafter, we used *AnaCOM2* available within the *BCBtoolkit* in order to perform Kruskal Wallis statistics (R Core Team 2016, <https://www.r-project.org>) on the disconnectome maps. *AnaCOM2* is comparable to *AnaCOM* (Kinkingnehun *et al.*, 2007) but has been reprogrammed and optimised to work on any Linux or Macintosh operating systems. *AnaCOM2* is a cluster-based lesion approach, which identifies the location of brain lesions that are associated with a given deficit, i.e. the regions that are critical for a given function. Compared to standard VLSM (Bates *et al.*, 2003), *AnaCOM2* regroups voxels with the same distribution of neuropsychological scores into clusters of voxels. Additionally, *AnaCOM2* performs non-parametric comparisons (Kruskal Wallis, Mann-Whitney or Kolmogorov-Smirnov) between patients and controls. Patients-controls comparison have been chosen as a first step in order to avoid drastic reduction of statistical power when two or more non-overlapping areas are responsible for patients reduced performance (Kinkingnehun *et al.*, 2007). Non-parametric statistics have been chosen as it is fair to consider that some clusters will not show a Gaussian distribution. *AnaCOM2* resulted in a statistical map that reveals, for each cluster, the significance of a deficit in patients undertaking a given task as compared to controls. Mann-Whitney between patients post-hoc comparisons were also performed in significant areas as post-hoc comparisons. Reported p-values were Bonferroni-Holm corrected for multiple comparisons (**Fig. 2**).

### *fMRI Meta-analyses*

A method described by Yarkoni *et al.* (2011; <http://neurosynth.org>) was used to identify the functional networks involved in category fluency. We searched for brain regions that are consistently activated in studies that load highly on 2 features: “fluency” (120 studies, 4214 activations) and “category” (287 studies, 10179 activations). The results were super-imposed on the 3D reconstruction of the MNI152 images (**Fig. 3**).

Running title: Advanced lesion symptom mapping analyses

### *Indirect disconnection of brain areas: functional connectivity network*

Rs-fMRI images were first motion corrected using MCFLIRT (Jenkinson *et al.*, 2002), then corrected for slice timing, smoothed with a full half width maximum equal to 1.5 times the largest voxel dimension and finally filtered for low temporal frequencies using a gaussian-weighted local fit to a straight line. These steps are available in Feat as part of FSL package (Woolrich *et al.*, 2009).

Rs-fMRI images were linearly registered to the enantiomorphic T1 images, and subsequently to the MNI152 template (2mm) using affine transformation. Confounding signals were discarded from rs-fMRI by regressing out a confound matrix from the functional data. The confound matrix included the estimated motion parameters obtained from the previously performed motion correction, the first eigenvariate of the white matter and cerebrospinal fluid as well as their first derivative. Eigenvariates can easily be extracted using `fslmeans` combined with the `--eig` option. White matter and cerebrospinal fluid eigenvariates were extracted using masks based on the T1 derived 3-classes segmentation thresholded to a probability value of 0.9, registered to the rs-fMRI images and binarized. Finally, the first derivative of the motion parameters, white matter and cerebrospinal fluid signal was calculated by linear convolution between their time course and a  $[-1 \ 0 \ 1]$  vector.

For each control participant, we extracted the time course that corresponded to each significant cluster and which was identified by the statistical analyses of the disconnectome maps. These time courses were subsequently correlated to the rest of the brain so as to extract seed-based resting-state networks. In order to obtain the most representative networks at the group level, for each seed-based resting-state network, we calculated the median network across the group. All these steps were automatized and made available as the *Funcon* tool as part of BCBtoolkit.

Visual inspection revealed that several of these resting state networks shared a very similar distribution of activations. Therefore, an ‘activation’ matrix was derived from the seed-based resting-state networks. This matrix consisted of columns that indicated each seed-based resting-state network, and rows that represented the level of activation for each voxel in the cortex. This ‘activation’ matrix was entered into a principal component analysis in SPSS (SPSS, Chicago, IL) using a covariance matrix and varimax rotation (with a maximum of 50 iterations for convergence), in order to estimate the number of principal components to

Running title: Advanced lesion symptom mapping analyses

extract for each function. Components were plotted according to their eigenvalue ( $y$ ) (Lower left panel in **Fig. 4**) and we applied a scree test to separate the principal from residual components. This analysis revealed that three factors were enough to explain 82% of the variance of the calculated seed-based resting-state networks. Finally, brain regions having a statistically significant relationship with the three components were detected using a linear regression with 5.000 permutations, in which the eigenvalues of the three components represented the independent variable and the seed-based resting-state networks the dependent variable. Results were Family Wise Error (FWE) corrected for multiple comparisons, and projected onto the average 3D rendering of the MNI152 template in the top panel of **Fig. 4**.

### *Structural changes in disconnected regions*

A distant lesion can affect cortical macro and microstructure remotely. Conscious of this, we attempted to estimate these structural changes and their relationship with category fluency within each functional network. To this aim, we explored the properties of each functional network using two complementary measures: T1w-based cortical thickness to identify fine local volumetric changes and the Shannon entropy of rs-fMRI as a surrogate for the local complexity of the neural networks (Tononi *et al.*, 1998). Each original functional network seeded from each cluster was thresholded and binarized at  $r > 0.3$  and used as mask to extract cortical thickness and entropy. Patients' lesions were masked out for these analyses.

For the cortical thickness, a registration-based method (Diffeomorphic Registration based Cortical Thickness, DiReCT) was employed (Das *et al.*, 2009) from the T1-weighted imaging dataset. The first step as for the *normalisation* was to produce an enantiomorphic filling of the damaged area in order to avoid the analysis to be contaminated by the lesioned tissue. The second step of this method consisted in creating two two-voxel thick sheets, one lying just between the grey matter and the white matter and the second lying between the grey matter and the cerebrospinal fluid. Then, the grey/white interface was expanded to the grey/cerebrospinal fluid interface using diffeomorphic deformation estimated with ANTs. The registration produced a correspondence field that allows an estimate of the distance between the grey/white and the grey/cerebrospinal fluid interfaces, and thus corresponded to an estimation of cortical thickness. Voxels belonging to the lesion were subsequently removed from the cortical thickness maps (see **supplementary figure 1**). This approach has good scan-rescan repeatability and good neurobiological validity as it can predict with a high

Running title: Advanced lesion symptom mapping analyses

statistical power the age and gender of the participants (Tustison *et al.*, 2014) as well as atrophy following brain lesions (Li *et al.*, 2015). Note that the striatum and the thalamus were excluded from the cortical thickness analysis since they do not have a cortical ribbon.

Shannon entropy was extracted from the previously preprocessed rs-fMRI using the following formula:  $-\sum(p \cdot \log(p))$  where  $p$  indicates the probability of the intensity in the voxels (Tononi *et al.*, 1998).

FSLstats was employed to extract the average cortical thickness and resting state fMRI entropy for each network. Statistical analysis was performed using SPSS software (SPSS, Chicago, IL). In our analysis, Gaussian distribution of the data was not confirmed for the cortical thickness and the entropy measures using the Shapiro–Wilk test. Therefore, Bivariate Spearman rank correlation coefficient analyses were performed between the cortical thickness or entropy measurement of each functional network and each patient’s category fluency performance. Correlation significant at  $P < 0.0041$  survives Bonferroni correction for multiple comparisons (12 networks).

## Results

### *White matter tracts disconnection*

Patients’ lesions were compared to an atlas of white matter connections in order to identify the probability of tract disconnections (Rojkova *et al.*, 2016). A Kruskal Wallis test indicated that for each tract, both preserved and disconnected, patients and control participants showed a significantly different performance on the category fluency test (all  $p < 0.001$ , full statistics reported in **Table 2**). Between patients, post-hoc comparisons revealed that disconnections of the left frontal aslant ( $U = 90$  ;  $p = 0.0389$ ), frontal inferior longitudinal ( $U = 69$  ;  $p = 0.0216$ ) and frontal superior longitudinal ( $U = 75$  ;  $p = 0.0352$ ) tracts, the anterior ( $U = 28.5$  ;  $p = 0.0116$ ) and long segment ( $U = 31.5$  ;  $p = 0.0059$ ) of the arcuate fasciculus were associated with a poorer performance in category fluency (**Fig. 1**). However, these post-hoc comparisons did not survive Bonferroni-Holm correction for multiple comparison.

These results indicate that poor performance measured in patients with brain damage can be associated to some extent with white matter tract disconnections.

Running title: Advanced lesion symptom mapping analyses

### *Direct disconnection of brain areas*

As the white matter tract disconnection approach cannot assess the disconnection of the subportion of tracts nor the involvement of multiple tracts by a lesion, data driven maps of disconnection or ‘disconnectomes’ were produced. Using tractography in a group of 10 healthy controls, the registered lesions were used as a seed to reveal white matter tracts that passed through the injured area so as to produce maps of disconnection, later referred to as disconnectome maps. Category fluency scores were attributed to each patient’s disconnectome map (see **Fig. 2a**). Results were further statistically assessed in order to identify areas that, when deafferented due to a disconnection mechanism, lead to a significant decrease in performance in category fluency when compared to controls.

The following results are Bonferroni-Holm corrected for multiple comparisons. Main cortical areas in the left hemisphere included the pre-supplementary motor area (Cluster size = 1449; Mann Whitney  $U = 88.5$  ;  $p = 0.025$ ), the anterior portion of the intraparietal sulcus (Cluster size = 1143;  $U = 18$  ;  $p = 0.030$ ), anterior (Cluster size = 837;  $U = 304$  ;  $p = 0.025$ ) and the middle (Cluster size = 898;  $U = 95.5$  ;  $p = 0.014$ ) cingulate gyrus, the middle frontal gyrus (Cluster size = 829;  $U = 81.5$  ;  $p = 0.005$ ), the pars opercularis of the inferior frontal gyrus (Cluster size = 5314;  $U = 16$  ;  $p = 0.025$ ).

In the right hemisphere the pre-supplementary motor area (Cluster size = 1050;  $U = 50.5$  ;  $p = 0.014$ ), the middle frontal gyrus (Cluster size = 552;  $U = 54$  ;  $p = 0.018$ ), the anterior (Cluster size = 572;  $U = 44.5$  ;  $p = 0.009$ ) and the middle (Cluster size = 817;  $U = 317$  ;  $p = 0.041$ ) cingulate gyrus were also involved (**Fig. 2b**)

Subcortical areas in the left hemisphere involved the caudate, the putamen and several ventral thalamic nuclei including the ventral anterior (VA), the ventrolateral anterior (VL<sub>a</sub>) and the ventrolateral posterior (VL<sub>p</sub>) as a part of the same cluster (Cluster size = 5314;  $U = 16$  ;  $p = 0.025$ )

In right hemisphere the caudate (Cluster size = 527;  $U = 310$  ;  $p = 0.031$ ) , the putamen (Cluster size = 1212;  $U = 225$  ;  $p = 0.033$ ) and the ventral thalamic nuclei (Cluster size = 935;

Running title: Advanced lesion symptom mapping analyses

$U = 202$  ;  $p = 0.025$ ) were similarly involved (**Fig. 2b**).

Additionally, between patients (i.e. connected and disconnected, Bonferroni-Holm corrected for multiple comparisons) comparisons confirmed the critical involvement of the preSMA ( $U = 88$ ,  $p = 0.0456$ ) the middle frontal gyrus ( $U = 75$ ,  $p = 0.0208$ ), the pars opercularis ( $U = 31$ ,  $p = 0.0132$ ) and the intra-parietal sulcus ( $U = 38$ ,  $p = 0.0245$ ) in the left hemisphere. The preSMA ( $U = 62$ ;  $p = 0.039$ ) was also involved in the right hemisphere (**Fig. 2c**).

Full statistics are reported in **Table 3**

### *fMRI Meta-analyses*

We further examined whether the disconnected areas in patients with poor performance are functionally engaged in tasks related to fluency and categorization using a meta-analysis approach (<http://neurosynth.org>) (Yarkoni *et al.*, 2011).

The result indicates that disconnected areas reported as significantly contributing to category fluency performance in patients are classically activated by functional MRI tasks requiring either fluency or categorization in healthy controls (**Fig. 3**).

### *Structural changes in disconnected regions*

Additional exploratory analyses investigated structural changes related to the disconnections. We estimated these changes using two complementary measures: T1w based cortical thickness to identify fine local volumetric changes and the Shannon entropy of rs-fMRI as a surrogate for the local complexity of the neural networks (Tononi *et al.*, 1998).

When compared to controls, patients showed a reduced cortical thickness in the left pars opercularis ( $H = 13$ ;  $p = 0.0012$ ), the middle frontal gyrus ( $H = 8$ ;  $p = 0.0143$ ), the pre-supplementary motor area ( $H = 8$ ;  $p = 0.0224$ ), the intraparietal sulcus ( $H = 9$ ;  $p = 0.0131$ ) and the right anterior ( $H = 7$  ;  $p = 0.0296$ ) and middle cingulate gyrus ( $H = 23$  ;  $p = 0.000$ ). When compared to patients with no disconnection, solely the right middle cingulate gyrus survived the Bonferroni-Holm correction for multiple comparison ( $U = 67$ ;  $p = 0.004$ ). When compared to controls, disconnected patients showed reduced entropy for all regions (all  $p <$

Running title: Advanced lesion symptom mapping analyses

0.05, except for right middle frontal gyrus). However, when compared to patients with no disconnection, none of the comparisons survived the Bonferroni-Holm correction for multiple comparisons. Uncorrected p values are reported as an indication in **table 4, and bar chart in supplementary figure 2.**

None of these measures correlated significantly with the fluency performance.

### *Indirect disconnection of brain areas*

As the disconnectome mapping method cannot measure the indirect disconnection produced by a lesion (i.e. it fails to measure the disconnection in a region that is not directly, anatomically connected to a damaged area, but that nonetheless remains a part of the same large network of functionally connected areas), we therefore employed functional connectivity in healthy controls. This allowed us to reveal the entire network of regions that are functionally connected to the areas that were reported as contributing significantly to the category fluency performance when directly disconnected. When compared to tractography, functional connectivity, has the added advantage of revealing the areas that contribute to the network through both direct, as well as indirect, structural connections.

Principal component analysis indicated that the significant areas contributing to category fluency performance belonged to 3 main functional networks (**Fig. 4**), which accounted for more than 80% of the total variance of the functional connectivity results.

The left cingulate clusters (anterior and middle), the right anterior cingulate, the middle frontal gyrus, the thalamus, and the operculum all belonged to the cingulo-opercular network (CO, Sadaghiani and D'Esposito, 2015) including also the right preSMA, posterior cingulate and the rostral portion of the middle frontal gyrus.

The middle of the cingulate gyrus and the striatum in the right hemisphere both belonged to a cortico-striatal network (CS, Voorn *et al.*, 2004) involving the right thalamus and striatum.

Finally, the left MFg, preSMA, IPs, the pars opercularis, the thalamus and the striatum were all involved in a larger, left ventral fronto-parietal network, which also included other areas such as the right preSMA, the frontal eye field and the temporo-parietal junction (VFP, Smith *et al.*, 2009).

Running title: Advanced lesion symptom mapping analyses

Additional analyses investigated the differences in the functional connectivity of these networks relative to the disconnected status of areas involved in category fluency. Between patients (i.e. connected and disconnected) comparisons revealed significantly lower functional connectivity in the left VFP network ( $U = 54$ ,  $p = 0.006$ ) and in the CS network ( $U = 63$ ,  $p = 0.027$ ) when anatomically disconnected. The CO network, however, did not show any significant difference ( $U = 40$ ,  $p = 0.213$ ). Moreover, the strength of the functional connectivity for each patient did not correlate significantly with the fluency performance.

In order to further assess the integrity of the whole network of regions that were functionally connected to the areas reported as having significantly contributed to the category fluency performance, we also extracted the cortical thickness and entropy from the regions that were functionally connected to the disconnected areas. Correlation analyses indicated that a thinner cortex in the ventral fronto-parietal network seeded from the left MFg (Spearman  $Rho = .464 \pm 0.341$ ;  $p = .004$ ), IPs ( $Rho = .475 \pm 0.341$ ;  $p = .003$ ) and left oper./striatum/thalamus ( $Rho = .512 \pm 0.341$ ;  $p = .001$ ) corresponded to a reduced performance in category fluency (**Fig. 5**). Additionally, a thinner cortical thickness in the left preSMA functional network ( $Rho = .376 \pm 0.341$ ;  $p = .024$ ) and a higher rs-fMRI entropy ( $Rho = -.420 \pm 0.370$ ;  $p = .019$ ) in the mid cingulate gyrus functional network was associated with poorer performance in category fluency. These two last results, however, did not survive Bonferroni-Holm correction for multiple comparisons.

## Discussion

A large set of complementary methods can capture the impact of lesions on distant regions and expose the subsequent consequences upon a patients' neuropsychological performance. Several of these methods are built directly into our freely available software package *BCBtoolkit*. This package can be employed to measure the pathophysiological mechanisms that cause cognitive deficits, and assess the relationship between these mechanisms and their consequential effect. Here we evaluated the risk of disconnection of classically defined white matter tracts and tested their relationship with category fluency performance. We then employed a tractography-based approach in order to reveal regions that were structurally

Running title: Advanced lesion symptom mapping analyses

disconnected by the lesion and assess their relationship with category fluency performance as compared to controls and other patients. Functional connectivity from the disconnected regions revealed large networks of interconnected areas. Within these regions/networks, measures of cortical thickness and of entropy of the rs-fMRI images were correlated to fluency performance, suggesting that some structural changes that occurred within these networks were due to the remote effect of a lesion that led to cognitive impairments. Consequently, the *BCBtoolkit* provided investigators with an ability to quantify the effect of brain damage upon the whole-brain, and explore its relationship to behavioural and cognitive abilities.

The investigation into the contribution of white matter tract disconnection is more than a century old approach and postulates an interruption in the course of white matter tracts in single case patients (Lichtheim, 1885; Catani and ffytche, 2005). Our method provides an anatomical rationale, as well as puts forth a statistical methodology enabling it to be extended to group-level studies. In the case of category fluency performance, this analysis particularly revealed a significant involvement of the anterior and long segments of the arcuate fasciculus, which are implicated in the language network (Catani and ffytche, 2005; Dronkers *et al.*, 2007; Forkel *et al.*, 2014). However, these tracts have been defined by their shape for convenience (e.g. uncinate for hook-shaped connections or arcuate for arched-shaped connections) and should not be considered as a single unit, as ultimately, sub-portions could contribute differently to the elaboration of the cognition and behaviour.

Data driven maps of disconnection or ‘disconnectomes’ were consequently produced in order to identify the sub-portion of disconnected tracts and reveal the pattern of cortico-subcortical areas that were disconnected by the lesion. For the first time, we exemplify that this method can go beyond assessing only lesions, and be employed to assess the relationship between disconnected areas and the patient’s neuropsychological performance. Here, this approach revealed that category fluency performance was significantly decreased, when several cortical and subcortical clusters were directly disconnected. The observed areas are consistent with previous lesion studies on fluency tasks (MacPherson *et al.*, 2015). Furthermore, each area identified as significantly involved in this analysis corresponded, almost systematically, to activation loci derived from fMRI studies in healthy controls performing fluency and/or

Running title: Advanced lesion symptom mapping analyses

categorisation tasks. This result suggests that the method appropriately identified altered functional networks contributing to the category fluency test. Nonetheless, one might argue that a cascade of polysynaptic events can influence behaviour and that dysfunctional, disconnected areas will also impact other indirectly connected areas.

In order to explore this additional dimension, we calculated the functional connectivity of the previously identified disconnected regions. In the case of the present analysis on category fluency performance, we revealed that the disconnected areas belonged to 3 large functional networks: a left dominant ventral fronto-parietal network, a mirror of the right-lateralized ventral attention network (Fox *et al.*, 2006), which link key language territories (Smith *et al.*, 2009) and is associated with executive functions (Power and Petersen, 2013; Parlatini *et al.*, 2017). We additionally showed the involvement of the cingulo-opercular network, a network that interacts with the fronto-parietal control network for the control of goal-directed behaviours (Gratton *et al.*, 2016), which together with cortico-striatal network may also be linked to a reduced performance in fluency tasks (Chouiter *et al.*, 2016). The cingulo-opercular and cortico-striatal networks may also have contributed to performance through the global inertia or the ability of participants to allocate and coordinate resources during the task (Bonnelle *et al.*, 2012). Finally, disconnection was associated with a significant reduction of functional connectivity in 2 out of the 3 networks investigated. This is an important result, as functional connectivity appeared to be less significantly impaired in bilateral networks, suggesting that the proportion of the preserved functional network in both of the intact hemispheres may contribute to the strength of functional connectivity.

Changes in connectivity should induce changes in the microstructure of the areas of projection, and provoke cognitive or behavioural consequences. Measures of the cortical thickness revealed a significant thinning for some, but not all, directly disconnected areas. This result may reflect a potential transneuronal degeneration mechanism (Fornito *et al.*, 2015). However, current limitations in spatial resolution and magnetic resonance imaging signal might have biased this measure in some regions due to changes in myelination in the lower layers of the cortex (Wagstyl *et al.*, 2015). Cortical thickness analyses revealed that the left dominant ventral fronto-parietal network, whether it is seeded from MFG, IPs or subcortical structures in the left hemisphere, had a reduced cortical thickness associated to the

Running title: Advanced lesion symptom mapping analyses

category fluency performance. This result indicates a strong and encouraging relationship between the integrity of a network derived from measures of cortical thickness and behavioural performances. Future research can benefit from this approach to stratify patients' population and predict potential recovery.

Additionally, we explored whether structural changes such as other neural (e.g. synaptic plasticity) or non-neural factors (e.g. altered properties of the vasculature) could also be captured by measures of rs-fMRI entropy, as a gauge to quantify the complexity of local blood oxygen level density (BOLD) across time. Although this was highly significant when patients were compared to controls, the result between patients (connected and disconnected patients) did not survive the correction for multiple comparisons, indicating that Shannon entropy measures of BOLD may be too noisy of a measure to capture such fine microstructural events with high statistical power.

Previous reports indicated that AnaCOM suffers from lower specificity than VLSM (Rorden *et al.*, 2009). AnaCOM compares patients with controls performances, an approach that has previously been criticised (Rorden *et al.*, 2009). In classical VLSM approaches, non-overlapping lesions are competing for statistical significance, fundamentally assuming that a single region is responsible for the symptoms. In the present study, we follow Associationist principles (Geschwind, 1965a, b) in assuming that several interconnected regions will contribute to the elaboration of the behaviour. By comparing the performance between patients and a control population using AnaCOM2, several non-overlapping regions can reach significance, without competing for it. Hence our results differ theoretically and methodologically from previous approaches. Perhaps more importantly, the network of disconnected areas revealed by AnaCOM2 is typically considered as functionally engaged for fluency and for categorization in healthy controls.

Newer multivariate methods have also been shown to provide superior performance compared to traditional VLSM (i.e. support vector regression lesion-symptom mapping, Mah *et al.*, 2014; Zhang *et al.*, 2014). For instance, such approaches have been employed to model the statistical relationship between damaged voxels in order to reduce false positives. In the disconnectome maps, this relationship has been pre-established using an anatomical prior derived from tractography in healthy controls. Therefore, it is not recommended to use

Running title: Advanced lesion symptom mapping analyses

multivariate approaches with the disconnectome maps, as they might come into conflict with the prebuilt anatomical association between the voxels. Additionally, these approaches require a much larger database of patients than the current study. Future research using large lesion databases will be required to explore the effect of multivariate statistical analysis on disconnectome maps.

Multivariate approaches also elegantly demonstrated that false positives can be driven by the vascular architecture (Mah *et al.*, 2014). This is an important limitation concerning any voxel and vascular lesion symptom mapping. Here, the group of patients explored included stroke and surgical lesions. Although we cannot exclude the participation of the vascular architecture in the present findings, the heterogeneity of the lesion included in our analyse may have limited this factor. Additionally, the statistical interaction between vascular architecture and the disconnectome map results remain to be explored in large database of lesions.

Methods used to estimate cortical thickness has previously been reported to perform poorly in peri-infarct regions, and the quality of the tissue segmentation may be particularly poor for stroke patients (Li *et al.*, 2015). Here, we followed previously published recommendations for applying DiReCT (Das *et al.*, 2009) to the data from stroke patients: the lesion was masked out, the tissue segmentations were visually inspected, and manual boundary correction was performed when necessary (see **supplementary figure 1** for an example).

Overall, using BCBtoolkit, researchers and clinicians can measure distant effects of brain lesions and associate these effects with neuropsychological outcomes. Taken together, these neuroimaging measures help discern the natural history of events occurring in the brain after a lesion, as well as assist in the localization of functions. These methods, gathered in the *BCBtoolkit*, are freely available as **supplementary software** at <http://toolkit.bcblab.com>

## Authors contribution

C.F. implemented the methods inside the BCBtoolkit, performed the analyses and wrote the manuscript. L.C. created the pipeline for the preprocessing of the resting state and for the

Running title: Advanced lesion symptom mapping analyses

functional correlation and revised the manuscript. S.K. conceived and help to upgrade the statistical analyses. C.R. collected the neuroimaging data. M.U. and E.V recruited the subjects, collected and built the database of patients and matched healthy controls including the neuropsychological and neuroimaging data and revised the manuscript. E.V. also participated in the conception of the lesion study, and also provided funding for the database acquisition. R.L. provided funding for the study and revised the manuscript. M.T.d.S. wrote the manuscript, provided funding, conceived and coordinated the study, reviewed and collected neuroimaging data.

## Acknowledgments

We thank Lauren Sakuma, Roberto Toro, Jean Dauniseau, Emmanuel Mandonnet, Beatrice Garcin, Stephanie J. Forkel and the BCBlab and Brainhack for useful discussions. The authors also thank the participants of this study as well as Prof. Claude Adam, Dr. Carole Azuar, Dr Marie-Laure Bréchemier, Dr. Dorian Chauvet, Dr Frédéric Clarençon Dr. Vincent Degos, Prof. Sophie Dupont, Prof. Damien Galanaud, Dr Béatrice Garcin, Dr. Florence Laigle, Dr Marc-Antoine Labeyrie, Dr. Anne Leger, Prof. Vincent Navarro, Prof. Pascale Pradat-Diehl, and Prof. Michel Wager for their help in recruiting the patients. The research leading to these results received funding from the “Agence Nationale de la Recherche” [grants number ANR-09-RPDOC-004-01 and number ANR-13- JSV4-0001-01] and from the Fondation pour la Recherche Médicale (FRM). Additional financial support comes from the program “Investissements d’avenir” ANR-10-IAIHU-06.

## References

- Avants BB, Tustison NJ, Song G, Cook PA, Klein A, Gee JC. A reproducible evaluation of ANTs similarity metric performance in brain image registration. *Neuroimage* 2011; 54(3): 2033-44.
- Badre D, Hoffman J, Cooney JW, D’Esposito M. Hierarchical cognitive control deficits following damage to the human frontal lobe. *Nat Neurosci* 2009; 12(4): 515-22.
- Bates E, Wilson S, Saygin A, Dick F, Sereno MI, Knight RT, *et al.* Voxel-based lesion-symptom mapping. *Nature Neuroscience* 2003; 6(5): 448-50.
- Bird CM, Malhotra P, Parton A, Coulthard E, Rushworth MF, Husain M. Visual neglect after right posterior cerebral artery infarction. *J Neurol Neurosurg Psychiatry* 2006; 77(9): 1008-12.

# Running title: Advanced lesion symptom mapping analyses

- Boes AD, Prasad S, Liu H, Liu Q, Pascual-Leone A, Caviness VS, Jr., *et al.* Network localization of neurological symptoms from focal brain lesions. *Brain* 2015; 138(Pt 10): 3061-75.
- Bonilha L, Jensen JH, Baker N, Breedlove J, Nesland T, Lin JJ, *et al.* The brain connectome as a personalized biomarker of seizure outcomes after temporal lobectomy. *Neurology* 2015; 84(18): 1846-53.
- Bonnelle V, Ham TE, Leech R, Kinnunen KM, Mehta MA, Greenwood RJ, *et al.* Salience network integrity predicts default mode network function after traumatic brain injury. *Proc Natl Acad Sci U S A* 2012; 109(12): 4690-5.
- Bredesen DE. Neural apoptosis. *Ann Neurol* 1995; 38(6): 839-51.
- Broca P. Perte de la parole, ramollissement chronique et destruction partielle du lobe antérieur gauche du cerveau. *Bull Soc Anthropol* 1861; 2: 235-8, 301-21.
- Capurso SA, Calhoun ME, Sukhov RR, Mouton PR, Price DL, Koliatsos VE. Deafferentation causes apoptosis in cortical sensory neurons in the adult rat. *J Neurosci* 1997; 17(19): 7372-84.
- Carrera E, Tononi G. Diaschisis: past, present, future. *Brain* 2014; 137(Pt 9): 2408-22.
- Catani M, Bambini V. A model for Social Communication And Language Evolution and Development (SCALED). *Curr Opin Neurobiol* 2014; 28: 165-71.
- Catani M, Dell'acqua F, Vergani F, Malik F, Hodge H, Roy P, *et al.* Short frontal lobe connections of the human brain. *Cortex* 2012; 48(2): 273-91.
- Catani M, ffytche DH. The rises and falls of disconnection syndromes. *Brain* 2005; 128(Pt 10): 2224-39.
- Catani M, Jones DK, ffytche DH. Perisylvian language networks of the human brain. *Annals of Neurology* 2005; 57(1): 8-16.
- Cazzoli D, Hopfner S, Preisig B, Zito G, Vanbellingen T, Jager M, *et al.* The influence of naturalistic, directionally non-specific motion on the spatial deployment of visual attention in right-hemispheric stroke. *Neuropsychologia* 2016; 92: 181-9.
- Chouiter L, Holmberg J, Manuel AL, Colombo F, Clarke S, Annoni JM, *et al.* Partly segregated cortico-subcortical pathways support phonologic and semantic verbal fluency: A lesion study. *Neuroscience* 2016; 329: 275-83.
- Ciccarelli O, Toosy AT, Parker GJ, Wheeler-Kingshott CA, Barker GJ, Miller DH, *et al.* Diffusion tractography based group mapping of major white-matter pathways in the human brain. *NeuroImage* 2003; 19(4): 1545-55.
- Corbetta M, Kincade MJ, Lewis C, Snyder AZ, Sapir A. Neural basis and recovery of spatial attention deficits in spatial neglect. *Nature Neuroscience* 2005; 8(11): 1603-10.
- Corbetta M, Ramsey L, Callejas A, Baldassarre A, Hacker CD, Siegel JS, *et al.* Common behavioral clusters and subcortical anatomy in stroke. *Neuron* 2015; 85(5): 927-41.
- Coulthard EJ, Nachev P, Husain M. Control over conflict during movement preparation: role of posterior parietal cortex. *Neuron* 2008; 58(1): 144-57.
- Cowan W. *Contemporary Research Methods in Neuroanatomy*: Springer; 1970.
- Damasio H, Damasio A. *Lesion analysis in Neuropsychology*. New York; 1989.
- Das SR, Avants BB, Grossman M, Gee JC. Registration based cortical thickness measurement. *Neuroimage* 2009; 45(3): 867-79.
- Dronkers NF, Plaisant O, Iba-Zizen MT, Cabanis EA. Paul Broca's historic cases: high resolution MR imaging of the brains of Leborgne and Lelong. *Brain* 2007; 130(Pt 5): 1432-41.
- Dronkers NF, Wilkins DP, Van Valin RD, Jr., Redfern BB, Jaeger JJ. Lesion analysis of the brain areas involved in language comprehension. *Cognition* 2004; 92(1-2): 145-77.

# Running title: Advanced lesion symptom mapping analyses

- Duffau H, Gatignol P, Mandonnet E, Peruzzi P, Tzourio-Mazoyer N, Capelle L. New insights into the anatomo-functional connectivity of the semantic system: a study using cortico-subcortical electrostimulations. *Brain* 2005; 128(Pt 4): 797-810.
- Feeney DM, Baron JC. Diaschisis. *Stroke* 1986; 17(5): 817-30.
- Finger S, Koehler PJ, Jagella C. The Monakow concept of diaschisis: origins and perspectives. *Arch Neurol* 2004; 61(2): 283-8.
- Forkel SJ, Thiebaut de Schotten M, Dell'Acqua F, Kalra L, Murphy DG, Williams SC, *et al.* Anatomical predictors of aphasia recovery: a tractography study of bilateral perisylvian language networks. *Brain* 2014; 137(Pt 7): 2027-39.
- Fornito A, Zalesky A, Breakspear M. The connectomics of brain disorders. *Nat Rev Neurosci* 2015; 16(3): 159-72.
- Fox MD, Corbetta M, Snyder A, Vincent JL, Raichle ME. Spontaneous neuronal activity distinguishes human dorsal and ventral attention systems. *Proc Natl Acad Sci USA* 2006; 103(26): 10046-51.
- Fridriksson J, Guo D, Fillmore P, Holland A, Rorden C. Damage to the anterior arcuate fasciculus predicts non-fluent speech production in aphasia. *Brain* 2013; 136(Pt 11): 3451-60.
- Geschwind N. Disconnexion syndromes in animals and man - Part I. *Brain* 1965a; 88: 237-94.
- Geschwind N. Disconnexion syndromes in animals and man - Part II. *Brain* 1965b; 88: 585-644.
- Gladsjo JA, Schuman CC, Evans JD, Peavy GM, Miller SW, Heaton RK. Norms for letter and category fluency: demographic corrections for age, education, and ethnicity. *Assessment* 1999; 6(2): 147-78.
- Gratton C, Neta M, Sun H, Ploran EJ, Schlaggar BL, Wheeler ME, *et al.* Distinct Stages of Moment-to-Moment Processing in the Cinguloopercular and Frontoparietal Networks. *Cereb Cortex* 2016.
- Griffis JC, Nenert R, Allendorfer JB, Szaflarski JP. Damage to white matter bottlenecks contributes to language impairments after left hemispheric stroke. *Neuroimage Clin* 2017; 14: 552-65.
- He BJ, Snyder A, Vincent JL, Epstein A, Shulman GL, Corbetta M. Breakdown of functional connectivity in frontoparietal networks underlies behavioral deficits in spatial neglect. *Neuron* 2007; 53(6): 905-18.
- Hope TM, Seghier ML, Prejawa S, Leff AP, Price CJ. Distinguishing the effect of lesion load from tract disconnection in the arcuate and uncinate fasciculi. *Neuroimage* 2016; 125: 1169-73.
- Husain M, Kennard C. Visual neglect associated with frontal lobe infarction. *J Neurol* 1996; 243(9): 652-7.
- Jenkinson M, Bannister P, Brady M, Smith S. Improved optimization for the robust and accurate linear registration and motion correction of brain images. *Neuroimage* 2002; 17(2): 825-41.
- Jones DK, Griffin LD, Alexander DC, Catani M, Horsfield MA, Howard RJ, *et al.* Spatial normalization and averaging of diffusion tensor MRI data sets. *NeuroImage* 2002; 17(2): 592-617.
- Jones DK, Simmons A, Williams SC, Horsfield MA. Non-invasive assessment of axonal fiber connectivity in the human brain via diffusion tensor MRI. *Magnetic Resonance in Medicine* 1999; 42(1): 37-41.

# Running title: Advanced lesion symptom mapping analyses

- Karnath HO, Ferber S, Himmelbach M. Spatial awareness is a function of the temporal not the posterior parietal lobe. *Nature* 2001; 411(6840): 950-3.
- Kinkingnehun S, Volle E, Pélérini-Issac M, Golmard JL, Lehericy S, du Boisguéheneuc F, *et al.* A novel approach to clinical-radiological correlations: Anatomico-Clinical Overlapping Maps (AnaCOM): method and validation. *NeuroImage* 2007; 37(4): 1237-49.
- Kuceyeski A, Navi BB, Kamel H, Raj A, Relkin N, Togliola J, *et al.* Structural connectome disruption at baseline predicts 6-months post-stroke outcome. *Hum Brain Mapp* 2016; 37(7): 2587-601.
- Lezak M. Neuropsychological assessment. Oxford: Oxford University Press; 1995.
- Li Q, Pardoe H, Lichter R, Werden E, Raffelt A, Cumming T, *et al.* Cortical thickness estimation in longitudinal stroke studies: A comparison of 3 measurement methods. *Neuroimage Clin* 2015; 8: 526-35.
- Lichtheim L. On aphasia. *Brain* 1885; 7: 433-84.
- Logothetis N. What we can do and what we cannot do with fMRI. *Nature* 2008; 453(7197): 869-78.
- MacPherson SE, Della Sala S. Handbook of Frontal Lobe Assessment. Oxford: Oxford University Press; 2015.
- MacPherson SE, Della Sala S, Cox S, Iveson MH. Handbook of Frontal Lobe Assessment. Oxford: Oxford University Press; 2015.
- Mah YH, Husain M, Rees G, Nachev P. Human brain lesion-deficit inference remapped. *Brain* 2014; 137(Pt 9): 2522-31.
- Mort DJ, Malhotra P, Mannan SK, Rorden C, Pambakian A, Kennard C, *et al.* The anatomy of visual neglect. *Brain* 2003; 126(Pt 9): 1986-97.
- Munafo M. Metascience: Reproducibility blues. *Nature* 2017; 543(7647): 619-20.
- Nachev P, Coulthard E, Jager HR, Kennard C, Husain M. Enantiomorphic normalization of focally lesioned brains. *Neuroimage* 2008; 39(3): 1215-26.
- Parlatini V, Radua J, Dell'Acqua F, Leslie A, Simmons A, Murphy DG, *et al.* Functional segregation and integration within fronto-parietal networks. *Neuroimage* 2017; 146: 367-75.
- Piai V, Meyer L, Dronkers NF, Knight RT. Neuroplasticity of language in left hemisphere stroke: evidence linking subsecond electrophysiology and structural connections. *Human Brain Mapping* 2017.
- Power JD, Petersen SE. Control-related systems in the human brain. *Curr Opin Neurobiol* 2013; 23(2): 223-8.
- Rojkova K, Volle E, Urbanski M, Humbert F, Dell'Acqua F, Thiebaut de Schotten M. Atlasing the frontal lobe connections and their variability due to age and education: a spherical deconvolution tractography study. *Brain Struct Funct* 2016; 221(3): 1751-66.
- Rorden C, Fridriksson J, Karnath HO. An evaluation of traditional and novel tools for lesion behavior mapping. *Neuroimage* 2009; 44(4): 1355-62.
- Rorden C, Karnath HO, Bonilha L. Improving lesion-symptom mapping. *J Cogn Neurosci* 2007; 19(7): 1081-8.
- Rudrauf D, Mehta S, Grabowski TJ. Disconnection's renaissance takes shape: Formal incorporation in group-level lesion studies. *Cortex* 2008; 44(8): 1084-96.
- Sadaghiani S, D'Esposito M. Functional Characterization of the Cingulo-Opercular Network in the Maintenance of Tonic Alertness. *Cereb Cortex* 2015; 25(9): 2763-73.
- Schaechter JD, Moore CI, Connell BD, Rosen BR, Dijkhuizen RM. Structural and functional plasticity in the somatosensory cortex of chronic stroke patients. *Brain* 2006; 129(Pt 10): 2722-33.
- Smith SM. Fast robust automated brain extraction. *Hum Brain Mapp* 2002; 17(3): 143-55.

Running title: Advanced lesion symptom mapping analyses

- Smith SM, Fox PT, Miller KL, Glahn DC, Fox PM, Mackay CE, *et al.* Correspondence of the brain's functional architecture during activation and rest. *Proc Natl Acad Sci U S A* 2009; 106(31): 13040-5.
- Thiebaut de Schotten M, Dell'Acqua F, Forkel SJ, Simmons A, Vergani F, Murphy DG, *et al.* A lateralized brain network for visuospatial attention. *Nat Neurosci* 2011a; 14(10): 1245-6.
- Thiebaut de Schotten M, Dell'Acqua F, Ratiu P, Leslie A, Howells H, Cabanis E, *et al.* From Phineas Gage and Monsieur Leborgne to H.M.: Revisiting Disconnection Syndromes. *Cereb Cortex* 2015; 25(12): 4812-27.
- Thiebaut de Schotten M, ffytche DH, Bizzi A, Dell'Acqua F, Allin M, Walshe M, *et al.* Atlasing location, asymmetry and inter-subject variability of white matter tracts in the human brain with MR diffusion tractography. *Neuroimage* 2011b; 54(1): 49-59.
- Thiebaut de Schotten M, Kinkingnehun S, Delmaire C, Lehericy S, Duffau H, Thivard L, *et al.* Visualization of disconnection syndromes in humans. *Cortex* 2008; 44(8): 1097-103.
- Thiebaut de Schotten M, Tomaiuolo F, Aiello M, Merola S, Silvetti M, Lecce F, *et al.* Damage to white matter pathways in subacute and chronic spatial neglect: a group study and 2 single-case studies with complete virtual "in vivo" tractography dissection. *Cereb Cortex* 2014; 24(3): 691-706.
- Tononi G, Edelman GM, Sporns O. Complexity and coherency: integrating information in the brain. *Trends Cogn Sci* 1998; 2(12): 474-84.
- Turken AU, Dronkers NF. The neural architecture of the language comprehension network: converging evidence from lesion and connectivity analyses. *Frontiers in systems neuroscience* 2011; 5: 1.
- Tustison NJ, Cook PA, Klein A, Song G, Das SR, Duda JT, *et al.* Large-scale evaluation of ANTs and FreeSurfer cortical thickness measurements. *Neuroimage* 2014; 99: 166-79.
- Urbanski M, Brechemier ML, Garcin B, Bendetowicz D, Thiebaut de Schotten M, Foulon C, *et al.* Reasoning by analogy requires the left frontal pole: lesion-deficit mapping and clinical implications. *Brain* 2016; 139(Pt 6): 1783-99.
- Volle E, Kinkingnehun S, Pochon JB, Mondon K, Thiebaut de Schotten M, Seassau M, *et al.* The functional architecture of the left posterior and lateral prefrontal cortex in humans. *Cereb Cortex* 2008; 18(10): 2460-9.
- Volle E, Levy R, Burgess PW. A new era for lesion-behavior mapping of prefrontal functions. In: D.T. S, Knight RT, editors. *Principles of Frontal Lobe Function*; 2013. p. 500-23.
- Von Der Heide RJ, Skipper LM, Klobusicky E, Olson IR. Dissecting the uncinate fasciculus: disorders, controversies and a hypothesis. *Brain* 2013; 136(Pt 6): 1692-707.
- Voorn P, Vanderschuren LJ, Groenewegen HJ, Robbins TW, Pennartz CM. Putting a spin on the dorsal-ventral divide of the striatum. *Trends Neurosci* 2004; 27(8): 468-74.
- Wagstyl K, Ronan L, Goodyer IM, Fletcher PC. Cortical thickness gradients in structural hierarchies. *Neuroimage* 2015; 111: 241-50.
- Woolrich MW, Jbabdi S, Patenaude B, Chappell M, Makni S, Behrens T, *et al.* Bayesian analysis of neuroimaging data in FSL. *Neuroimage* 2009; 45(1 Suppl): S173-86.
- Xing S, Lacey EH, Skipper-Kallal LM, Jiang X, Harris-Love ML, Zeng J, *et al.* Right hemisphere grey matter structure and language outcomes in chronic left hemisphere stroke. *Brain* 2016; 139(Pt 1): 227-41.
- Yarkoni T, Poldrack RA, Nichols TE, Van Essen DC, Wager TD. Large-scale automated synthesis of human functional neuroimaging data. *Nat Methods* 2011; 8(8): 665-70.

Running title: Advanced lesion symptom mapping analyses

Yourganov G, Fridriksson J, Rorden C, Gleichgerrcht E, Bonilha L. Multivariate Connectome-Based Symptom Mapping in Post-Stroke Patients: Networks Supporting Language and Speech. *J Neurosci* 2016; 36(25): 6668-79.

Zhang Y, Brady M, Smith SM. Segmentation of brain MR images through a hidden Markov random field model and the expectation-maximization algorithm. *IEEE Trans Med Imaging* 2001; 20: 45–57.

Zhang Y, Kimberg DY, Coslett HB, Schwartz MF, Wang Z. Multivariate lesion-symptom mapping using support vector regression. *Hum Brain Mapp* 2014; 35(12): 5861-76.

## Captions

**Fig. 1:** Category fluency performance (mean performance with 95% confidence intervals) for patients with (dark grey) or without (light grey) disconnection of each tract of interest. The green intervals indicate the range of controls performance corresponding to 95% confidence intervals. \*  $p < 0.05$

**Fig. 2:** Areas directly disconnected by the lesion that significantly contributed to a decreased score on category fluency task (referred to as “disconnected areas” in the manuscript). a) Representative slices from disconnectome maps computed for category fluency performance, blue clusters indicate group average low performance and red high performance. b) Brain areas contributing significantly after correction for multiple comparison. c) Category fluency performance (mean performance with 95% confidence intervals) for patients with (dark grey) or without (light grey) disconnection of each of the examined cortical regions. The green interval indicates performance in matched controls with 95% confidence intervals. preSMA: presupplementary motor area, IPs: intraparietal sulcus, MFg: middle frontal gyrus, pars Op.: frontal pars opercularis, A: anterior group of thalamic nuclei, VA ventral anterior VLp: ventrolateral posterior, VLa: ventrolateral anterior. \*  $p < 0.05$  Bonferroni-Holms corrected for multiple comparisons.

**Fig. 3:** Areas classically activated with fMRI ( $p < 0.01$  FDR corrected) during fluency (pink) and categorization (cyan) tasks. Areas involved in both fluency and categorization are highlighted in dark blue.

**Fig. 4:** Functional networks involving the identified disconnected areas, as defined by resting

Running title: Advanced lesion symptom mapping analyses

state functional connectivity. Top panel, main cortical networks involving the disconnected areas revealed by a principal component analysis. Bottom left panel, principal component analysis of the raw functional connectivity result. Bottom right panel, strength of the functional connectivity for patients with (dark grey) or without (light grey) involvement of the functional network. CO: Cingulo-opercular network, CS: cortico-striatal network, VFP: Ventral fronto-parietal network. \* indicates  $p < 0.05$ ; \*\*,  $p < 0.01$

**Fig. 5:** Dimensional relationship between cortical thickness measured in rs-fMRI disconnected networks and category fluency. Note that regression lines (in black) and intervals (mean confidence intervals in red) are for illustrative purposes since we performed a rank-order correlation.

Running title: Advanced lesion symptom mapping analyses

**Table 1:** Demographical and clinical data

ID	Age (years)	Education (years)	Gender	Lesion side	Lesion volume (mm <sup>3</sup> )	Lesion delay (months)	Aetiology
P01	56	17	F	right	255	7	stroke
P02	55	19	M	left	34374	76	hematoma
P03	46	17	F	left	14847	126	stroke
P04	50	11	F	left	110145		surgery
P05	64	14	M	right	59048	119	stroke
P06	32	16	F	right	15946	129	epilepsy
P07	51	11	M	bilateral	113170		stroke
P08	70	5	F	left	51530	85	surgery
P09	47	11	M	right	7809	115	hematoma
P10	62	13	F	bilateral	21295	14	hematoma
P11	41	16	M	right	55848	29	surgery
P12	46	12	M	bilateral	2542	51	hematoma
P13	67	15	M	left	4102	133	stroke
P14	49	9	M	bilateral	14929	19	hematoma
P15	36	14	F	right	40854	82	surgery
P16	40	22	F	left	24829	56	hematoma
P17	40	14	M	bilateral	14364	7	hematoma
P18	23	16	F	right	21681	47	surgery
P19	54	22	M	right	51897	48	stroke
P20	71	17	M	left	25779	91	hematoma
P21	23	15	F	right	29513	36	surgery
P22	27	9	F	left	12986	30	surgery
P23	26	13	F	left	2640	19	surgery
P24	32	14	F	left	12653	4	surgery
P25	59	16	F	left	97	9	hematoma
P26	26	13	F	left	26928		stroke
P27	58	12	M	left	1026	3	stroke
P29	75	12	F	left	14938	16	hematoma
P30	52	13	F	right	11978	20	surgery
P31	58	12	M	right	13263	21	surgery

# Running title: Advanced lesion symptom mapping analyses

P32	62	5	M	right	20281	9	surgery
P33	41	17	M	left	7463	29	surgery
P34	42	17	M	left	24319	6	Infection
P35	60	12	M	right	41897	24	surgery
P36	51	14	F	right	39213	17	surgery
P37	51	12	F	right	8133	48	surgery
P38	33	17	M	right	140947	48	surgery

Running title: Advanced lesion symptom mapping analyses

**Table 2:** White matter tracts disconnection relationship with category fluency statistical report. Results are Bonferroni-Holms corrected for multiple comparisons. n1, number of patients disconnected; n2, number of patients spared

Tracts	3 groups comparison		Patients disconnected and connected		Patients disconnected and controls		Patients connected and controls		n1	n2
	K	P value	U	P value	U	P value	U	P value		
Cingulum Left	19	0.0001	141	0.2035	189	0.0003	277	0.0003	16	21
Cingulum Right	19	0.0001	161	0.5	280	0.0001	187	0.0019	23	14
Uncinate Left	19	0.0001	148	0.3994	176	0.0027	291	0.0001	13	24
Uncinate Right	19	0.0001	167	0.4635	209	0.0004	258	0.0003	17	20
Arcuate Anterior Segment Left	22	0.0000	29	0.0116	12	0.0004	454	0.0001	5	32
Arcuate Anterior Segment Right	19	0.0001	126	0.3855	118	0.0025	348	0.0001	16	21
Arcuate Long Segment Left	23	0.0000	32	0.0059	13	0.0001	453	0.0002	6	31
Arcuate Long Segment Right	19	0.0001	107	0.2559	117	0.0068	349	0.0001	9	28
Inferior Fronto Occipital fasciculus Left	19	0.0001	165	0.5	196	0.0011	271	0.0001	15	22
Inferior Fronto Occipital fasciculus Right	19	0.0001	157	0.3457	199	0.0002	268	0.0004	17	20
Frontal Aslant Tract Left	21	0.0000	90	0.0389	90	0.0001	377	0.0004	11	26
Frontal Aslant tract Right	19	0.0001	155	0.3131	194	0.0001	272	0.0012	18	19
Frontal Inferior Longitudinal Left	21	0.0000	69	0.0216	54	0.0001	413	0.0004	9	28
Frontal Inferior Longitudinal Right	19	0.0001	140	0.3051	171	0.0022	295	0.0001	13	34
Frontal Superior Longitudinal Left	20	0.0000	75	0.0352	73	0.0004	393	0.0002	9	28
Frontal Superior Longitudinal Right	19	0.0001	129	0.1992	120	0.0001	346	0.0005	13	34

Running title: Advanced lesion symptom mapping analyses

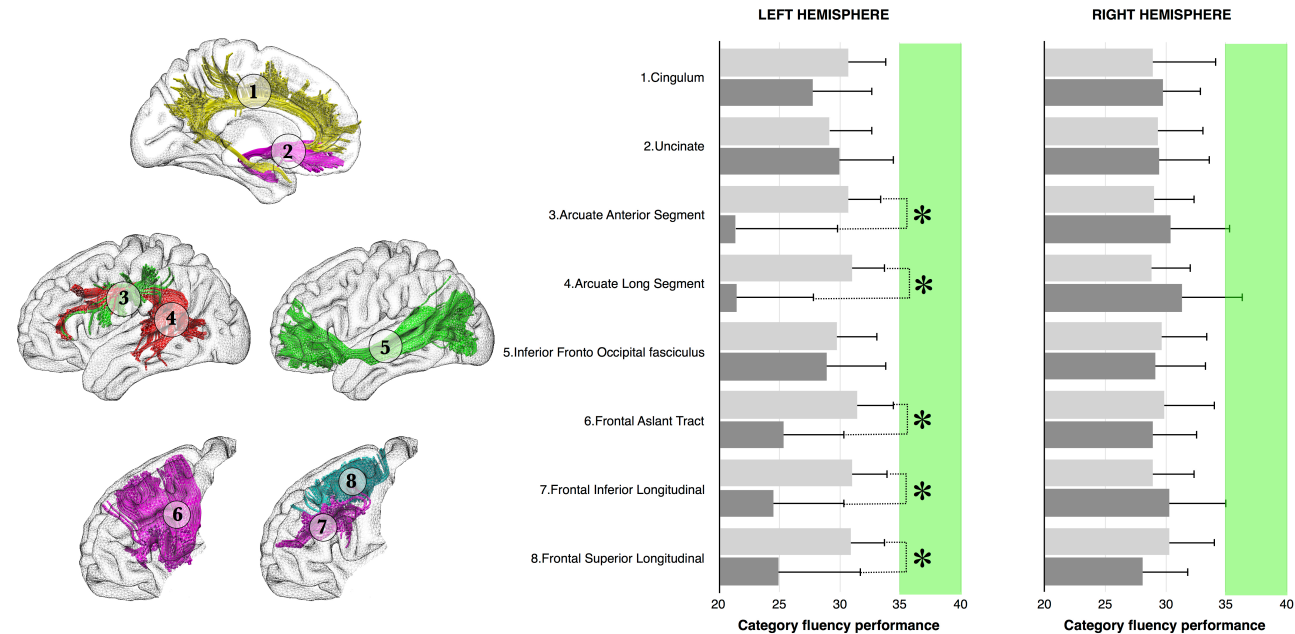
**Table 3:** Direct disconnection of brain areas relationship with category fluency statistical report. Results are Bonferroni-Holms corrected for multiple comparisons. n1, number of patients disconnected; n2, number of patients spared

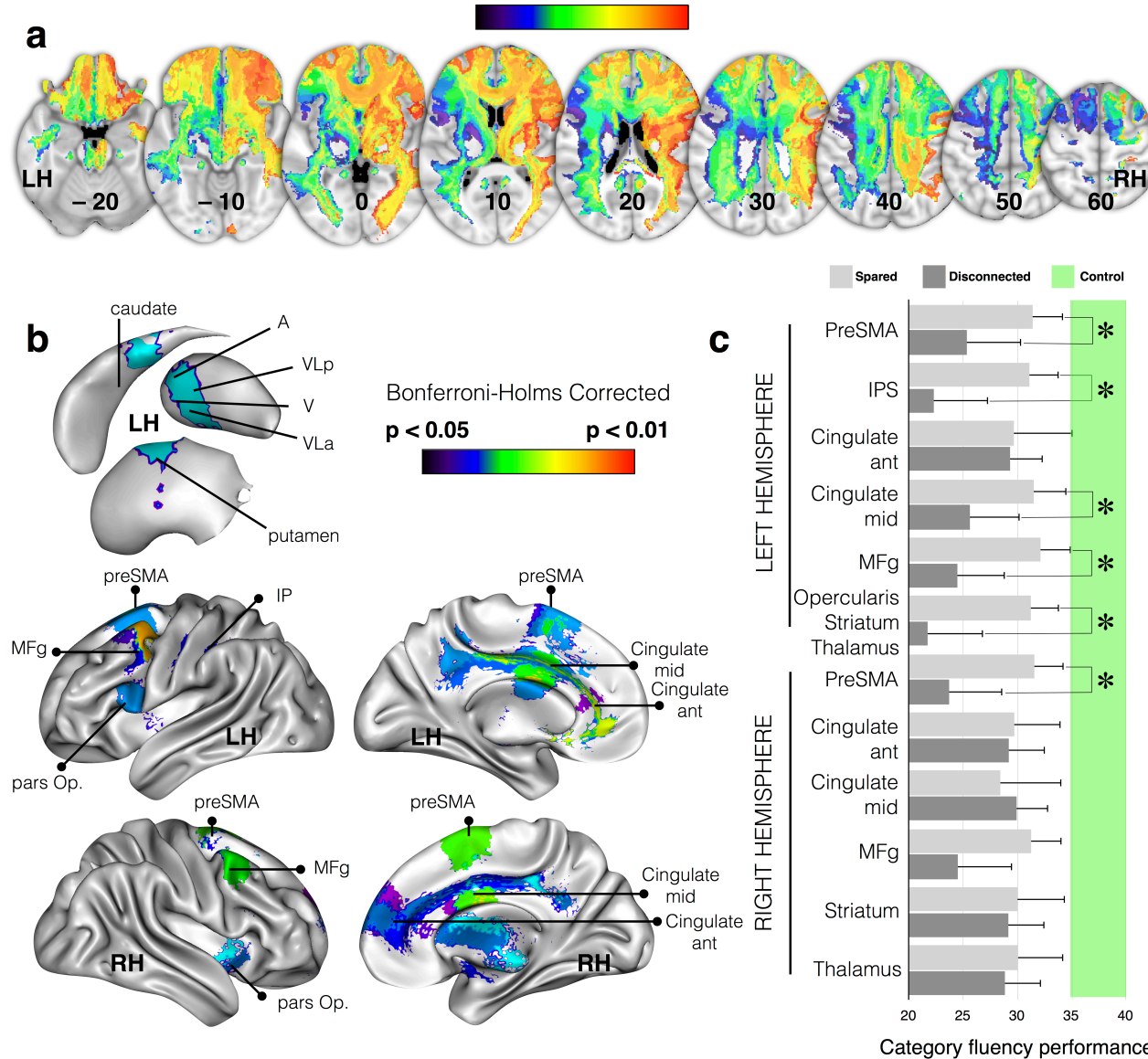
		3 groups comparison		Patients disconnected and connected		Patients disconnected and controls		Patients connected and controls		n1	n2
	Disconnected areas	K	P value	U	P value	U	P value	U	P value		
FLUENCY SCORE LEFT HEMISPHERE	PreSMA	18.6697	0.0001	139.5	0.3726	304	0.0000	139.5	0.3726	12	25
	IPs	18.8698	0.0001	154.5	0.3235	225	0.0001	154.5	0.3235	7	30
	Cingulate ant	21.5229	0.0000	93	0.0232	95.5	0.0000	93	0.0232	25	12
	Cingulate mid	18.6268	0.0001	137.5	0.3483	317	0.0001	137.5	0.3483	13	24
	MFg	23.3510	0.0000	38	0.0049	18	0.0001	38	0.0049	13	24
	Opercularis	23.1283	0.0000	75	0.0052	81.5	0.0000	75	0.0052	7	30
FLUENCY SCORE RIGHT HEMISPHERE	PreSMA	22.0686	0.0000	74	0.0191	54	0.0000	74	0.0191	10	27
	Cingulate ant	23.9965	0.0000	31	0.0022	16	0.0000	31	0.0022	20	17
	Cingulate mid	21.3413	0.0000	88	0.0228	88.5	0.0000	88	0.0228	25	12
	MFg	22.9272	0.0000	62	0.0065	50.5	0.0000	62	0.0065	10	27

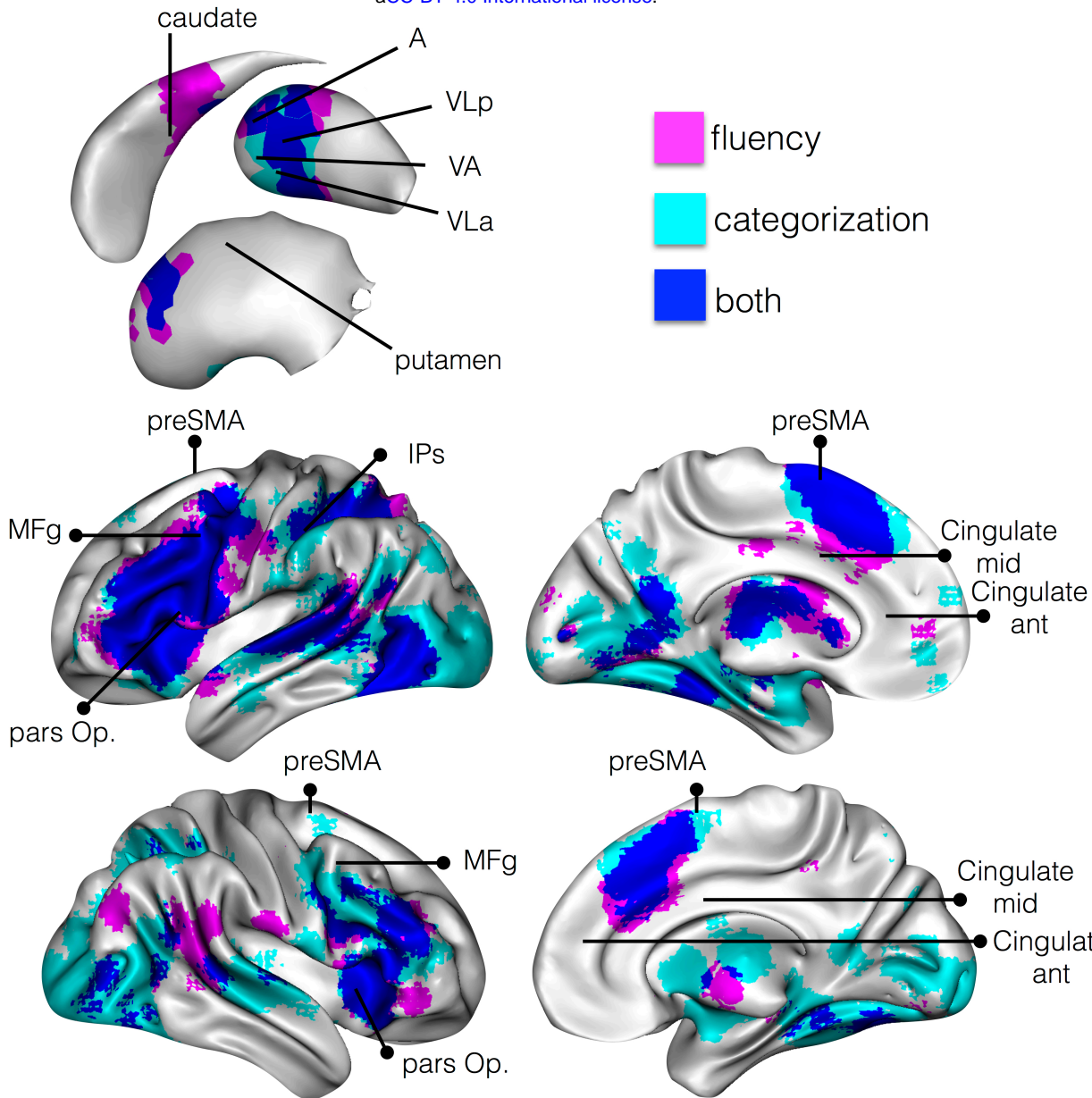
Running title: Advanced lesion symptom mapping analyses

**Table 4:** Cortical thickness and fMRI entropy measures in disconnected areas. Uncorrected P values. n1, number of patients disconnected; n2, number of patients spared

		3 groups comparison		Patients disconnected and connected		Patients disconnected and controls		Patients connected and controls		n1	n2
	Disconnected areas	Kruskal Wallis	P value	U	P value	U	P value	U	P value		
CORTICAL THICKNESS LEFT HEMISPHERE	PreSMA	8	0.0224	109	0.0944	168	0.0057	514	0.0565	12	25
	IPs	9	0.0131	54	0.0251	59	0.0019	667	0.1134	7	30
	Cingulate ant	5	0.0822	110	0.1000	465	0.0175	269	0.2061	25	12
	Cingulate mid	5	0.0759	139	0.2998	278	0.1436	435	0.0137	13	24
	MFg	8	0.0143	109	0.0695	172	0.0028	502	0.0710	13	24
	Opercularis	13	0.0012	40	0.0061	44	0.0006	583	0.0225	7	30
CORTICAL THICKNESS RIGHT HEMISPHERE	PreSMA	4	0.1328	134	0.4931	214	0.1711	523	0.0254	10	27
	Cingulate ant	7	0.0296	167	0.4696	362	0.0191	295	0.0169	20	17
	Cingulate mid	23	0.0000	61	0.0020	223	0.1414	254	0.1415	25	12
	MFg	6	0.0587	116	0.2634	163	0.0359	538	0.0359	10	27
SHANNON ENTROPY LEFT HEMISPHERE	PreSMA	24	0.0000	86	0.2171	85	0.0004	210	0.0000	12	25
	IPs	27	0.0000	40	0.0422	18	0.0002	260	0.0000	7	30
	Cingulate ant	44	0.0000	84	0.1158	109	0.0000	3	0.0000	25	12
	Cingulate mid	36	0.0000	97	0.3029	45	0.0000	127	0.0000	13	24
	MFg	16	0.0004	100	0.4246	125	0.0043	272	0.0003	13	24
	Opercularis, striatum, thalamus	17	0.0002	65	0.3680	75	0.0181	287	0.0001	7	30
SHANNON ENTROPY RIGHT HEMISPHERE	PreSMA	8	0.0177	82	0.2364	117	0.0078	413	0.0243	10	27
	Cingulate ant	55	0.0000	81	0.0640	16	0.0000	4	0.0000	20	17
	Cingulate mid	22	0.0000	111	0.4596	203	0.0001	114	0.0003	25	12
	MFg	22	0.0000	55	0.0497	136	0.0533	209	0.0000	10	27
	Striatum	23	0.0000	110	0.4436	202	0.0001	100	0.0001	14	23
	Thalamus	58	0.0000	67	0.0204	0	0.0000	6	0.0000	14	23







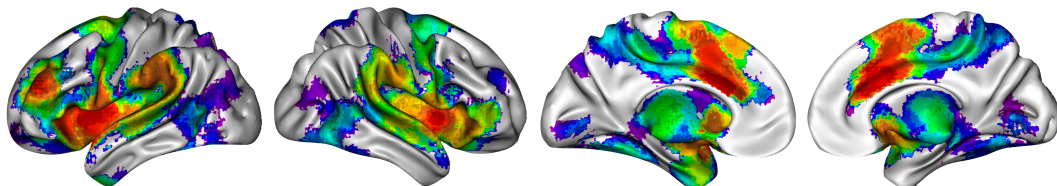
p values (FWE corrected)

0.05

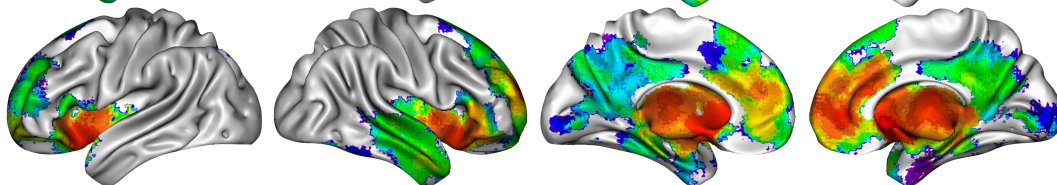
0.001



CO



CS



VFP

